Research Article Vol. 29, No. 5 / 1 March 2021 / Optics Express 6330
Optics EXPRESS

Pre-chirp managed divided-pulse amplification using composite birefringent plates for pulse division and recombination: en route toward GW peak power

RUNZHI CHEN[1,2] AND GUOQING CHANG[1,2,*]

[1]Beijing National Laboratory for Condensed Matter Physics, Institute of Physics, Chinese Academy of Sciences, Beijing 100190, China
[2]University of Chinese Academy of Sciences, Beijing 100049, China
[*]guoqing.chang@iphy.ac.cn

Abstract: Pre-chirp managed amplification (PCMA) allows the generation of optical pulses with a duration well below 100 fs. However, the pulse peak power is limited to <50 MW due to poor energy scalability. In this paper, we combine PCMA and divided pulse amplification to overcome this bottleneck. The resulting pre-chirp managed divided-pulse amplification (PCM-DPA) employs birefringent plates as the pulse divider/recombiner thanks to the picosecond pulse duration in the amplifier. Our numerical analysis shows that the group-delay dispersion (GDD) difference among pulse replicas results in reduced combining efficiency with increased replica numbers. We propose using composite birefringent plates to construct the divider/recombiner that features negligible GDD-difference. An Yb-fiber PCM-DPA system incorporating such composite-plate based divider/recombiner for 64 replicas can produce 121-μJ, 44-fs pulses with 2.3-GW peak power. To have a compact system, we further propose a hybrid design which can deliver 61-μJ, 48-fs pulses with 1.13-GW peak power. These results represent >30 times improvement in both pulse energy and peak power compared with current Yb-fiber PCMA systems.

1. Introduction

To date, most high power Yb-fiber laser systems are configured in the architecture of master-oscillator-power-amplifier [1]. To prevent degradation of pulse quality caused by fiber nonlinearity, chirped-pulse amplification (CPA) has been widely adopted in Yb-fiber amplifiers [2–4]. In a typical fiber CPA system, the seeding pulses produced by a master oscillator are stretched to >100 ps, then amplified in Yb-fibers, and finally compressed by a pulse compressor. The use of Yb-fibers with large mode area in a CPA system allows generation of 800-fs pulses with 71-W average power and 1.45-mJ pulse energy [5]. In an Yb-fiber CPA system, the gain bandwidth limits the compressed pulses to a typical value of >200 fs in duration. Some applications (e.g., cavity-enhanced high-harmonic generation) demand much shorter pulse duration (well below 100 fs) with pulse energies at micro-joule level. These pulses can be generated by post compressing the ~200-fs pulses produced by a fiber CPA system at the expense of system complexity. An alternative is to utilize nonlinear amplification methods, in which the optical spectrum of the amplified pulses is significantly broadened well beyond the gain bandwidth of the Yb-fiber amplifier; as a result, the amplified pulses can be compressed to well below 100 fs. To date, three nonlinear amplification techniques have been developed for fiber amplifiers, i.e., parabolic pulse amplification [6–9], pre-chirp managed amplification (PCMA) [10–19], and gain-managed amplification [20,21]. In a PCMA system, the seeding pulses are properly pre-chirped prior to amplification, and a joint optimization of both the pre-chirper and the compressor allows generation of μJ-level femtosecond pulses with tens of fs duration [13–15,17,19]. Especially,

#414309 https://doi.org/10.1364/OE.414309
Journal © 2021 Received 6 Nov 2020; revised 12 Jan 2021; accepted 12 Jan 2021; published 16 Feb 2021

Optics EXPRESS

by further optimization of the central wavelength and pulse energy in the main amplifier, 24-fs pulses are obtained in an Yb-fiber PCMA system [16].

Although nonlinear amplification methods lead to much shorter pulse duration, the resulting pulse energies are much lower than can be achieved from an Yb-fiber CPA system. The highest pulse energy from a nonlinear Yb-fiber amplifier is 2 μJ produced by PCMA seeded by circularly polarized pulses [19]. Further energy scaling is limited by the onset of self-focusing, which has a threshold of 4 MW (6 MW) for linearly (circularly) polarized pulses. Given that the amplified pulses are about 1 ps in duration, the maximum pulse energy is thus limited to several micro-joule.

In this paper, we propose pre-chirp managed divided-pulse amplification (PCM-DPA) that combines PCMA and divided pulse amplification (DPA) to overcome the bottleneck of energy scalability in the current PCMA technique. Thanks to the picosecond pulse duration in a PCMA system, birefringent plates can be employed as the pulse divider and recombiner. Using birefringent plates can avoid spatially splitting the optical beam and therefore ensure the system simplicity since active stabilization is not necessary. In this paper, we present a systematic investigation on the energy scalability of PCM-DPA by carefully analyzing the effects of the group-delay (GD) difference and group-delay dispersion (GDD) difference among pulse replicas. Indeed, Florent Guichard *et al*. has analyzed DPA in Yb-fiber parabolic amplifiers and found that the coherent combining efficiency drops quickly with an increased number of pulse replicas due to the accumulated GDD difference [22]. To mitigate this general limit imposed to divided-pulse nonlinear fiber amplifiers, we propose to use composite birefringent plates to construct the divider/recombiner. As an example, a composite plate may include an YVO4 plate and an α-BBO plate with their optical axes aligned in the same direction and their thickness ratio set at 1:4. A divider/recombiner constructed from such composite plates features negligible GDD difference among pulse replicas and therefore allows nearly 100% combining efficiency for 64 replicas in an Yb-fiber PCM-DPA system. To implement a compact system, we further propose a hybrid design, in which the GDD difference in a divider/recombiner is partially compensated. Nevertheless, this hybrid design for 32 replicas allows us to generate 61-μJ, 48-fs pulses with 1.13-GW peak power, representing >30 times peak-power improvement than can be achieved in current PCMA systems.

2. Concept and modeling of PCM-DPA

Figure 1 illustrates the general configuration of an Yb-fiber PCM-DPA system. Linearly polarized pulses emitted from the laser frontend are pre-chirped by a pair of diffraction-gratings. The divider includes m sets of half-wave plates (HWPs) and birefringent crystals and splits each pre-chirped pulse into 2^m identical replicas. The n^{th} crystal has the twice thickness of the $(n-1)^{th}$ one. To facilitate energy scaling, a quarter-wave plate (QWP) converts these replicas from linear polarization into circular polarization before they are coupled into an Yb-fiber amplifier. As we have shown recently, seeding PCMA by circularly polarized pulses improves the amplified pulse energy by a factor of 1.5 [19]. After the amplifier, another QWP converts the amplified replicas back to linear polarization before entering the recombiner. The recombiner includes identical components of the divider but they are arranged in the reversed order. A polarizer is added at the output of the recombiner to extract the combined pulse while rejecting the uncombined part. The amplified 2^m replicas are assembled into one pulse by the recombiner and then compressed by a compressor, which may be based on high-dispersion chirped mirrors or another pair of diffraction-gratings.

Ultrafast pulses in the PCM-DPA system can be represented by a vector $\boldsymbol{A}$ with two orthogonally polarized modes: $\boldsymbol{A} = \hat{e}_x A_x + \hat{e}_y A_y$, where $\hat{e}_x$ and $\hat{e}_y$ denote the two orthogonal eigenvectors. A_x and A_y stand for amplitudes of the corresponding polarization components. The seeding pulse $\boldsymbol{A}_0$ produced by the laser frontend is assumed to be x-polarized (i.e., $A_{0y} = 0$). We add a quadratic phase to the optical spectrum of A_{0x} to model the pulse that passes through the pre-chirping device (e.g., a pair of diffraction gratings) prior to the pulse division. Pulse division is achieved

Optics EXPRESS

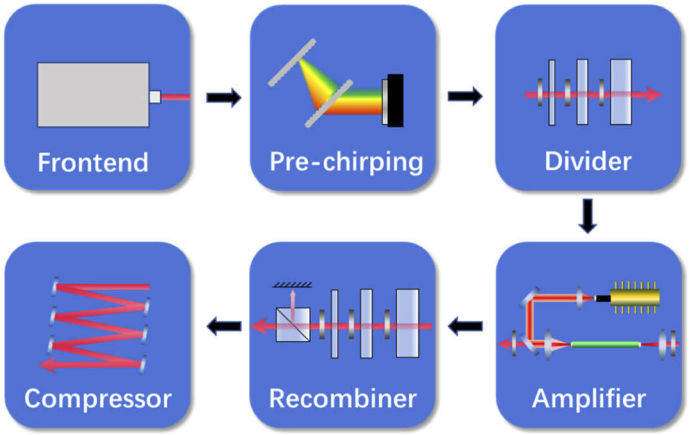

Fig. 1. Schematic of Yb-fiber PCM-DPA system including six parts: laser frontend, pre-chirping device, divider, amplifier, recombiner, and compressor.

by HWPs and birefringent crystals (Fig. 2). To split the seeding pulse into 2^m replicas, m sets of HWPs and birefringent crystals are required. After the first HWP, the input polarization is rotated and aligned at 45° with respect to the x-axis such that the x-polarized and y-polarized components have equal amplitudes (i.e., $A'_{0x} = A'_{0y}$). In practice, birefringent plates made of uniaxial crystals are employed to construct the divider/recombiner. For the sake of simplicity, we assume that x-polarized replicas correspond to ordinary wave (o-wave) and y-polarized replicas extraordinary wave (e-wave). Therefore A'_{0x} and A'_{0y} experience different refractive indices of n_o and n_e, respectively, which results in two temporally separated replicas, A_{1x} and A_{1y}.

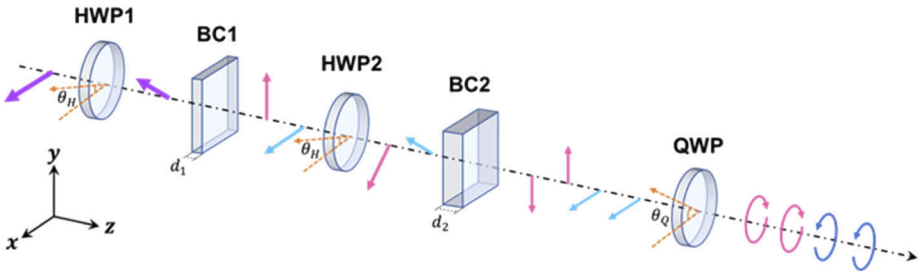

Fig. 2. Schematic of pulse division for m=2. HWP: half-wave plate, BC: birefringent crystal, QWP: quarter-wave plate.

As Fig. 2 shows, one HWP and one birefringent plate perform one division. The k-th ($1 \le k \le m$) pulse division can be found by the following iterative process:

(1) The k-th HWP alters the polarization direction of 2^{k-1} replicas of $\boldsymbol{A}_{k-1}$, which can be represented by a Jones matrix that acts on $\boldsymbol{A}_{k-1}$,

$$\begin{bmatrix} A'_{(k-1)x} \\ A'_{(k-1)y} \end{bmatrix} = e^{-\frac{i\pi}{2}} \begin{bmatrix} \cos^2\theta_H - \sin^2\theta_H & 2\cos\theta_H \sin\theta_H \\ 2\cos\theta_H \sin\theta_H & \sin^2\theta_H - \cos^2\theta_H \end{bmatrix} \begin{bmatrix} A_{(k-1)x} \\ A_{(k-1)y} \end{bmatrix} \tag{1}$$

θ_H represents the angle between fast axis and x-axis and is set at 22.5°.

Optics EXPRESS

(2) Each replica of A'_{k-1} is further split into two replicas by the k-th birefringent crystal. The resulting $\boldsymbol{A}_k$ can be easily calculated by

$$A_{kx} = \frac{1}{2\pi}\int_{-\infty}^{\infty} \tilde{A}'_{(k-1)x}\exp\left(\frac{n_o\omega d_k}{c} - i\omega T\right)\mathrm{d}\omega \tag{2}$$

$$A_{ky} = \frac{1}{2\pi}\int_{-\infty}^{\infty} \tilde{A}'_{(k-1)y}\exp\left(\frac{n_e\omega d_k}{c} - i\omega T\right)\mathrm{d}\omega \tag{3}$$

where $\tilde{A}$ denotes the Fourier transform of A. c is the light speed in vacuum and d_k is the thickness of the k-th birefringent crystal. A_{kx} (A_{ky}) represents 2^{k-1} x(y)-polarized pulse replicas. To make these replicas equally spaced in time, d_k=2d_{k-1} is satisfied. The plate is placed at the normal incidence to avoid beam walk-off. The refractive indices of the o-wave replica (n_o) and e-wave replica (n_e) can be calculated from their Sellmeier equations.

Before coupling the 2^m pulse replicas into the Yb-fiber amplifier, we transform these linearly polarized replicas to their circular polarization counterparts. This process is achieved using a QWP (See Fig. 2) and can be modeled by the following Jones calculus:

$$\begin{bmatrix} A_x(z=0) \\ A_y(z=0) \end{bmatrix} = \mathrm{e}^{-\frac{i\pi}{4}} \begin{bmatrix} \cos^2\theta_Q + i\sin^2\theta_Q & (1-i)\sin\theta_Q\cos\theta_Q \\ (1-i)\sin\theta_Q\cos\theta_Q & \sin^2\theta_Q + i\cos^2\theta_Q \end{bmatrix} \begin{bmatrix} A_{mx} \\ A_{my} \end{bmatrix} \tag{4}$$

θ_Q is set at 45°, and thus $\boldsymbol{A}$(z=0) represents the resulting 2^m circularly polarized pulse replicas.

Nonlinear fiber amplification of the pulse replicas is modeled by coupled generalized nonlinear Schrödinger equations (CGNLSE) [23]

$$\frac{\partial A_+}{\partial z} + \sum_{n\geq 2}\frac{i^{n+1}\beta_n}{n!}\frac{\partial^n A_+}{\partial T^n} = \gamma\left(i - \frac{1}{\omega_0}\frac{\partial}{\partial T}\right)\left(f_R A_+ \int_{-\infty}^{+\infty} h_R(T-t')[|A_+(t')|^2 + |A_-(t')|^2]dt' + (1-f_R)A_+\left[\frac{2}{3}|A_+|^2 + \frac{4}{3}|A_-|^2\right]\right) + \frac{(1+\alpha i)g}{2}A_+ \tag{5}$$

$$\frac{\partial A_-}{\partial z} + \sum_{n\geq 2}\frac{i^{n+1}\beta_n}{n!}\frac{\partial^n A_-}{\partial T^n} = \gamma\left(i - \frac{1}{\omega_0}\frac{\partial}{\partial T}\right)\left(f_R A_- \int_{-\infty}^{+\infty} h_R(T-t')[|A_-(t')|^2 + |A_+(t')|^2]dt' + (1-f_R)A_-\left[\frac{2}{3}|A_-|^2 + \frac{4}{3}|A_+|^2\right]\right) + \frac{(1+\alpha i)g}{2}A_- \tag{6}$$

A_+ and A_- represent the complex amplitudes of the right-handed circular polarization eigenstate and left-handed circular polarization eigenstate, respectively. They are related to A_x and A_y by

$$\begin{bmatrix} A_+ \\ A_- \end{bmatrix} = \frac{1}{\sqrt{2}}\begin{bmatrix} 1 & i \\ 1 & -i \end{bmatrix}\begin{bmatrix} A_x \\ A_y \end{bmatrix} \tag{7}$$

γ is the nonlinear parameter defined as $\gamma=\omega_0 n_2/cA_{eff}$. ω_0 is the center frequency, n_2 the nonlinear-index coefficient, and A_{eff} the mode-field area. $f_R = 0.18$ denotes the fractional contribution of the Raman response and $h_R(t)$ is the Raman response function. g in the last term on the right-hand side represents the gain coefficient of the fiber amplifier and α is the amplitude-phase coupling constant derived from Kramers-Kronig relations. Gain saturation is included using the local Frantz-Nodvik equation [24]

$$g(z,T) = g_0\exp\left(-\frac{\int_{-\infty}^{T}|A_+(z,t')|^2 + |A_-(z,t')|^2dt'}{E_{sat}}\right) \tag{8}$$

where g_0 is the small signal gain and E_{sat} the saturation energy of the fiber amplifier. It is noteworthy that our modeling neglects the dependence of fiber-amplifier gain on frequency. Nevertheless, our previous investigation has verified its validity of reliably reproducing the experimental results [19].

Optics EXPRESS

After the amplification, all the circularly polarized replicas are converted back to linear polarization by another QWP, and then recombined by the same HWPs and crystals, which corresponds to calculating Eqs. (1), (2), (3) and (4) in a reversed order without changing any parameters. The pulse compression is modeled as removing the quadratic phase of the optical spectrum of the recombined pulse.

3. PCM-DPA based on single-material (i.e., YVO_4 or α-BBO) birefringent plates for pulse division and recombination

Birefringent-plate based divider and recombiner have been widely used for energy scaling in the context of pulse amplification, pulse compression, and fiber oscillator [22,25–34]. To date, all the demonstrated divider/recombiner employ birefringent plates of single material. For example, YVO_4 (positive uniaxial crystal) birefringent plates have become the popular choice when incorporating DPA into Yb-fiber amplifiers. When an YVO_4 birefringent plate splits an input pulse into two orthogonally polarized replicas, the refractive-index difference between the o-wave and the e-wave imposes different amount of GD and GDD to the two replicas. This GD difference renders temporal delay between the two replicas and the GDD difference makes their pulse profiles differ from each other in terms of duration and peak power. An YVO_4 plate of 1-mm in thickness generates 748-fs GD difference and 91.2-fs^2 GDD difference, respectively. When constructing a divider for a PCMA system that involves accumulation of tremendous nonlinear phase shift, the crystal thickness should be large enough such that the adjacent replicas are well temporally separated to avoid detrimental nonlinear interaction. To illustrate the effect of replica overlapping on pulse recombination and compression, we simulate an Yb-fiber PCM-DPA system in which an input pulse is split into two replicas by one YVO_4 plate. In the simulation, the input pulse is obtained by adding −50000 fs^2 GDD to a 300-fs transform-limited Gaussian pulse centered at 1036 nm. Table 1 lists the simulation parameters for modeling the PCM-DPA system. We assume that each replica has an input energy of 65 nJ and is amplified to 2.05 μJ if gain saturation is absent. These parameters have been demonstrated in our recent experimental work [19].

Table 1. Parameters in the simulation for modeling PCM-DPA system

Input pulse	
Center wavelength	1036 nm
Spectral profile	Gaussian
Spectral bandwidth (FWHM)	5.3 nm @ 1036 nm
GDD added to the optical spectrum for pre-chirping the input pulse	−50000 fs^2
Pulse duration (negatively pre-chirped)	551 fs
Power amplifier (from NKT, aeroGAIN-ROD)	
Fiber length	80 cm
Fiber mode-field diameter (MFD)	65 μm
Small signal gain, g_0	0.0432 cm^{-1}
Amplitude-phase coupling constant, α	1
Saturation energy, E_{sat}	1.05 mJ
Group-velocity dispersion, β_2	20 fs^2/mm
Third-order dispersion, β_3	40 fs^3/mm
Nonlinear refractive index, n_2	2.6×10^{-20} m^2/W

In the first simulation, we set the thickness of the YVO_4 plate at 1 mm such that the two orthogonally polarized replicas are separated by 748 fs. As shown in Fig. 3(a), these two replicas

Optics EXPRESS

have considerable temporal overlap and share the same optical spectrum [inset of Fig. 3(a)]. During the subsequent amplification in the Yb-fiber amplifier, this temporal overlap causes strong cross-phase modulation (XPM) that significantly reshapes the pulse profiles of the two replicas and their spectra [Fig. 3(b)]. Clearly these two amplified replicas are substantially different in terms of temporal profile and optical spectrum, resulting in poor recombination. The black curve in Fig. 3(c) shows the recombined pulse after the polarizer in the recombiner. The XPM imposes complicated nonlinear phase to the trailing (leading) edge of the o-wave (e-wave) replica; as a result, the compressed pulse [blue curve in Fig. 3(c)] has two satellite lobes including about half of the pulse energy. The pulse has a duration of 50 fs with 17.6-MW peak power. For comparison, the red dotted curve represents twice the compressed pulse generated from the Yb-fiber PCMA system seeded by one single replica. In other words, the red dotted curve corresponds to the ideal compressed pulse delivered by such a PCM-DPA system with a perfect combination. As expected, temporal overlap leads to degraded compressed pulse with poor recombining efficiency.

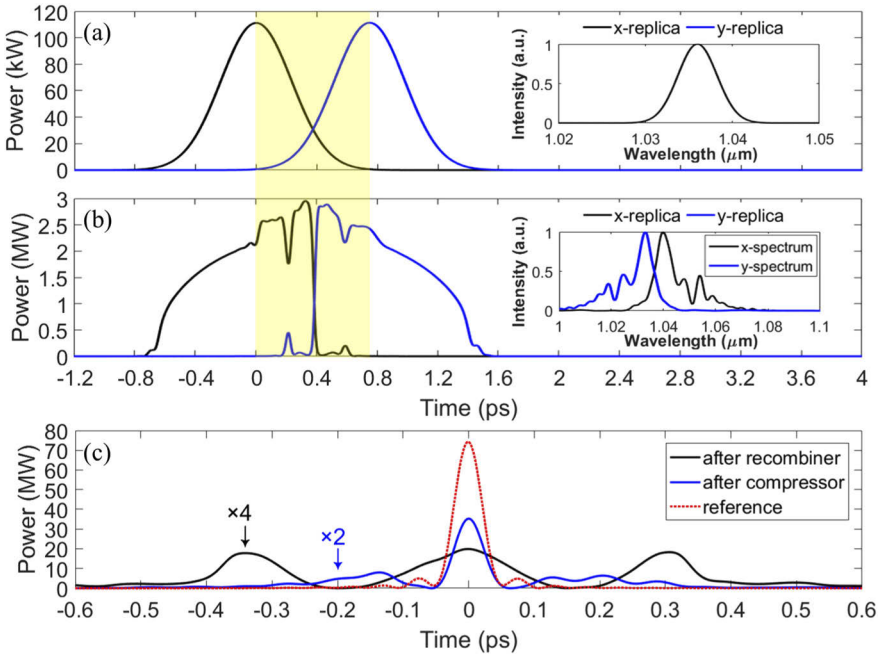

Fig. 3. Simulation results for amplifying two replicas with 1-mm YVO_4 plate as the divider/recombiner. (a) Two replicas after the divider. Inset: optical spectrum of the replicas. (b) Two replicas after amplification with their spectra shown as inset. (c) Pulse recombination and compression. Black curve: pulse after recombiner, blue curve: compressed pulse, and red dotted curve: twice the compressed pulse produced by the single-replica seeded PCMA.

To show the effect of the GDD difference and make a comparison with the results in Fig. 3, we redo the simulation in which the YVO_4 thickness is set at 2 cm. Due to an increased GD difference, the two replicas after the divider are well separated by ~15 ps as shown in Fig. 4(a). The 2-cm YVO_4 generates 1824-fs^2 GDD-difference between the two replicas, which in turn introduces noticeable difference to the replicas in terms of pulse duration (522 fs for x-replica and 506 fs for y-replica) and peak power (117.3 kW for x-replica and 120.5 kW for y-replica). At the amplifier output, the pulse duration and peak power of x-replica (y-replica) are 1164 fs (1158 fs) and 1.937 MW (1.932 MW) [Fig. 4(b)]. Figure 4(c) shows the pulse after the recombiner (black curve), the compressed pulse (blue curve), and twice the compressed pulse corresponding to single replica case (red dotted curve), respectively. The compressed pulse has a duration of

Optics EXPRESS

62 fs with 51.6-MW peak power. Compared with the results shown in Fig. 3(c), increasing the YVO_4 thickness from 1 mm to 2 cm significantly improves the compressed pulse quality and the recombining efficiency. Nevertheless, the considerable deviation between the blue curve and the red dotted curve suggests that the combining efficiency can be further improved.

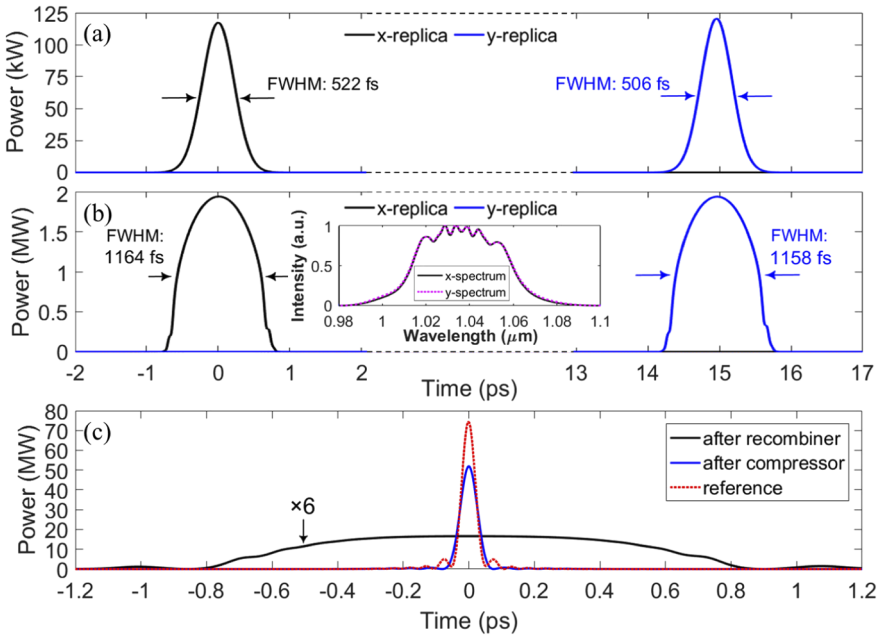

Fig. 4. Simulation results for amplifying two replicas with 2-cm YVO_4 plate as the divider/recombiner. (a) Two replicas after the divider. (b) Two replicas after amplification with their spectra shown as inset. (c) Pulse recombination and compression. Black curve: pulse after recombiner, blue curve: compressed pulse, and red dotted curve: twice the compressed pulse produced by the single-replica seeded PCMA.

The results in Fig. 3 and Fig. 4 indicate that the YVO_4 thickness plays an essential role and should be optimized such that the PCM-DPA achieves the best performance. One might use combining efficiency to quantify the system performance. Reference [22] defines a total combining efficiency η as the product between spatial combining efficiency $\eta_{spatial}$ and temporal combining efficiency $\eta_{temporal}$

$$\eta = \eta_{spatial} \times \eta_{temporal} \tag{9}$$

$\eta_{spatial}$ is given by

$$\eta_{spatial} = \frac{E_{combined}}{E_{combined} + E_{uncombined}} \tag{10}$$

where $E_{combined}$ denotes the recombined pulse energy passing through the polarizer and $E_{uncombined}$ corresponds to the uncombined fraction that is rejected by the polarizer. $\eta_{temporal}$ can be calculated by

$$\eta_{temporal} = \frac{\int_{-\Delta\tau/2}^{\Delta\tau/2} |A_{combined}(t)|^2 dt}{\int_{-\infty}^{\infty} |A_{combined}(t)|^2 dt} \tag{11}$$

where $A_{combined}$ represents the complex amplitude of the recombined pulse calculated after the compression and $\Delta\tau$ denotes the interval between the adjacent replicas during amplification. $\eta_{temporal}$ actually depicts how much energy is concentrated in the main peak of the recombined pulse.

Optics EXPRESS

Figure 5 plots the total combining efficiency as a function of the thickness of the first YVO_4 plate for different number of replicas. The solid and dotted curves correspond to the simulation results with and without gain saturation effect included, respectively. The results in Fig. 5 reveal four universal features in a PCM-DPA system:

(1) Given a fixed replica number, a maximum combining efficiency exists. For example, as the two replicas are generated by an YVO_4 plate of 1.7-mm thick, the combining efficiency reaches the highest 99%. The duration of the replica pulses changes from 550 fs at the amplifier input to 1174 fs at the amplifier output. Therefore the 1272-fs separation given by the 1.7-mm thick YVO_4 plate guarantees a minimal temporal overlap between the two replicas during the amplification.

(2) As exemplified by the results in Fig. 3 and Fig. 4, the combining efficiency is limited by the temporal overlap (GDD difference) as the YVO_4 is too thin (thick). The optimum thickness to achieve the maximum combining efficiency corresponds to a tradeoff between minimizing the temporal overlap and minimizing the GDD difference. As the replica number increases, the GDD difference becomes more prominent and, consequently, the optimum thickness of the first YVO_4 decreases.

(3) The maximum combining efficiency decreases as the replica number increases largely because the GDD difference grows rapidly as well. For 64 replicas, the combining efficiency is 76% corresponding to the optimum thickness of the first YVO_4 plate at 1.2 mm.

(4) The effect of gain saturation becomes more significant as the replica number increases. For 64 replicas, gain saturation accounts for ~7% extra decrease of the combining efficiency.

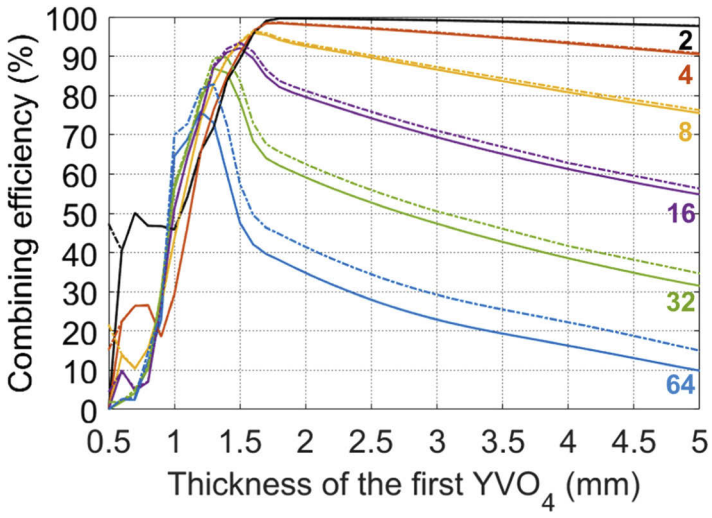

Fig. 5. Combining efficiency versus thickness of the first YVO_4 for different number of replicas. Solid curves and dashed curves correspond to simulation results with gain saturation and without gain saturation, respectively.

In many applications, the pulse peak power rather than pulse energy determines the system performance. Figure 6(a) plots the compressed pulse peak power with respect to the thickness of the first YVO_4 plate for different number of replicas. As we increase the replica number, the maximum pulse peak power increases while the optimum thickness of the first YVO_4 plate decreases. For 64 replicas, the maximum peak power is 0.67 GW and the optimum thickness is

Optics EXPRESS

1.4 mm, which differs from the predicted thickness of 1.2 mm that corresponds to the highest combining efficiency (blue curve in Fig. 5). The black curve in the inset of Fig. 6(a) shows the compressed pulse, and the red dotted curve presents 64 times the compressed pulse produced by the single-replica seeded PCMA as the reference pulse. Clearly the compressed pulse is far from the perfect case: although the combining efficiency surpasses 70%, the peak power of the compressed pulse is only about one quarter of the peak power of the reference pulse. The results indicate that the combining efficiency does not directly relate to pulse peak power and may not be an appropriate measure to evaluate the system performance. In this paper, we propose the following figure of merit (FOM) to evaluate the performance of a PCM-DPA system:

$$FOM = \frac{P_{compressed}}{P_{reference}} \tag{12}$$

$P_{compressed}$ denotes the peak power of the compressed pulse given by the PCM-DPA using 2^m replicas and $P_{reference}$ represents 2^m times the peak power of a single replica seeded PCMA. This FOM can simply assess the overall effects of the pulse combination and compression. Figure 6(b) shows the FOM as a function of the thickness of the first YVO_4 plate for variant replica numbers. Compared with the combining efficiency defined by Eq. (11), the proposed FOM is more sensitive to the GDD difference among these replicas such that the optimum FOM rapidly decreases from 1.01 to 0.26 as the replica number varies from 2 to 64. For 32 and 64 replicas, FOM stays below 0.5 indicating that scaling the peak power by doubling the number of divided replicas becomes unacceptably inefficient. It is noteworthy that the optimum FOM for 2 and 4 replicas may exceed 1. This is because small XPM caused by slight temporal overlap among the replicas may result in favorable phase to the amplified spectra such that the compressed pulse from a PCM-DPA system has a shorter duration and higher peak power, which leads to a FOM slightly exceeding 1.

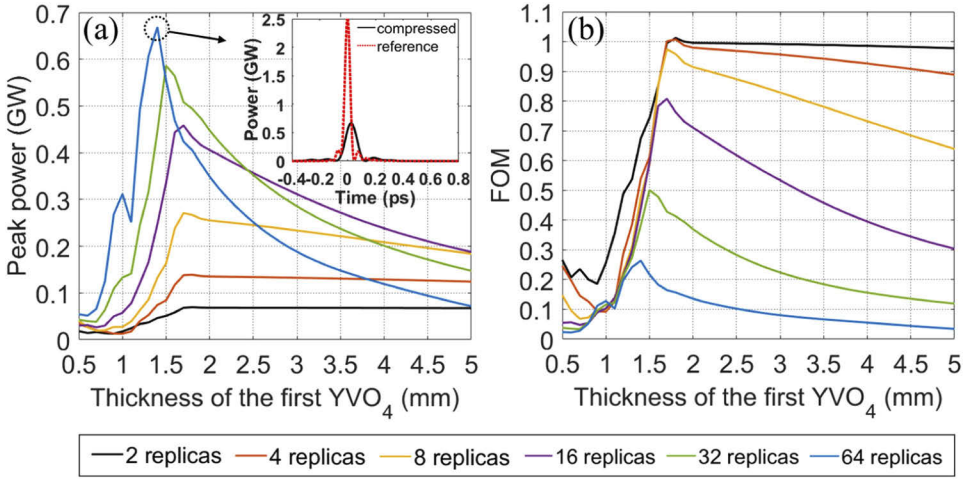

Fig. 6. (a) Peak power and (b) FOM of the compressed pulse generated by our PCM-DPA system based on YVO_4 plates for different replica numbers. Inset: the compressed pulse (black curve) and corresponding reference pulse (red dotted curve) at the optimum plate-thickness of 1.4 mm for 64 replicas.

The results in Fig. 5 and Fig. 6 immediately suggest that the GDD difference among the pulse replicas limits the energy/power scalability of a PCM-DPA system. It is thus anticipated that reducing the replica GDD-difference may improve the system performance. To confirm this speculation, we replace YVO_4 plates by α-BBO (negative uniaxial crystal) plates in our simulation. The GD difference and GDD difference of 1-mm thick α-BBO is 464 fs and 21.5

Optics EXPRESS

fs^2, respectively. In other words, a 1.6-mm-thick α-BBO plate and a 1-mm-thick YVO_4 plate generate the same amount of temporal delay (i.e., 748 fs) between the two orthogonally polarized replicas; however, the α-BBO plate results in a GDD difference of only 34.7-fs^2, less than half of that given by the YVO_4 plate. As Fig. 7 shows, switching to α-BBO plates significantly improves both the optimum peak power and FOM corresponding to large number (>16) of replicas. For 64 replicas, as the first α-BBO is 2.6 mm in thickness, the peak power attains 1.25 GW [inset in Fig. 7(a)] corresponding to an optimum FOM more than 0.5 [blue curve in Fig. 7(b)].

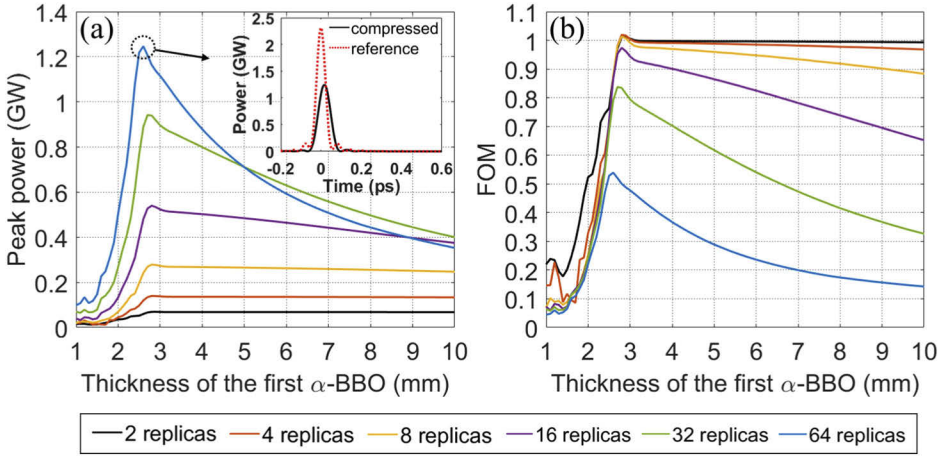

Fig. 7. (a) Peak power and (b) FOM of the compressed pulse generated by our PCM-DPA system based on α-BBO plates for different replica numbers. Inset: the compressed pulse (black curve) and corresponding reference pulse (red dotted curve) at the optimum plate-thickness of 2.6 mm for 64 replicas.

4. PCM-DPA based on dual-material (i.e., YVO_4 and BBO) birefringent plates for pulse division and combination

The results in Fig. 6(a) show that the peak power obtained using 64 replicas drops rapidly as the thickness deviates from 1.4 mm. When the thickness is large than 1.5 mm, the peak power resulted from 64 replicas becomes less than that from 32 replicas. Even using the α-BBO plates with less GDD-difference, the peak power for 64 replicas becomes lower than that of 32-replicas case when the thickness of the first plate exceeds 5 mm [blue curve in Fig. 7(a)]; for 64 replicas, FOM more than 0.5 merely exists in the small thickness range of 2.5–2.8 mm [blue curve in Fig. 7(b)]. These results convincingly indicate that the excessive GDD-difference degrades the energy scaling of an Yb-fiber PCM-DPA system. To remove such a restriction, we propose using composite birefringent plates to construct the divider/recombiner. As the inset of Fig. 8(a) shows, each composite plate includes an YVO_4 plate and an α-BBO plate with their optical axes aligned in the same direction. To minimize the GDD difference associated with such a composite plate, we set the thickness of α-BBO plate four times that of YVO_4 plate. Figure 8(a) shows the wavelength-dependent GDD difference for 1-mm YVO_4 plate (blue curve), 1-mm α-BBO plate (red curve), and 1-mm composite plate (black curve). The GD difference of 1-mm composite plate is 221.6 fs while the GDD difference is only 1.04 fs^2 at 1036 nm. Furthermore, the composite GDD difference stays below 2 fs^2 in the wavelength range of 0.98–1.1 μm.

Figure 8(b) plots the combining efficiency as a function of the thickness of the first composite plate for different replica numbers. The combining efficiency for ≤32 replicas increases to nearly 100% as the first composite plate is 6-mm thick. Thanks to the negligible GDD-difference, further increasing the thickness to 10 mm does not compromise the combining efficiency, which leads to

Optics EXPRESS

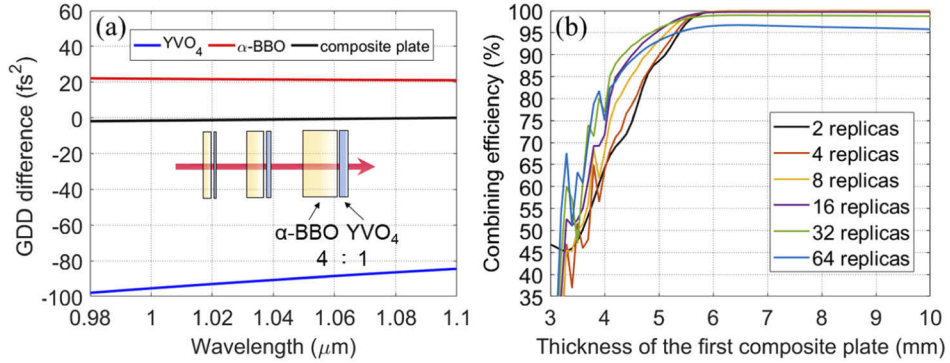

Fig. 8. (a) Wavelength-dependent GDD difference of 1-mm YVO_4 (blue curve), α-BBO (red curve), and the composite plate (black curve). (b) Combining efficiency versus thickness of the first composite plate for different number of replicas.

a broader thickness range for achieving high combining efficiency. The adverse effect caused by the GDD difference becomes severe for 64 replicas [blue curve in Fig. 8(b)]; nevertheless, the combining efficiency remains at ~96% as the thickness of the first composite plate varies in the range of 6–10 mm.

Figure 9 shows the peak power [Fig. 9(a)] and FOM [Fig. 9(b)] of the compressed pulses. The PCM-DPA system using 32 replicas can deliver compressed pulses with >1.2-GW peak power [green curve in Fig. 9(a)], which outperforms the case of 64 replicas employing single material (YVO4 or α-BBO) plates. The results in Fig. 9(b) show that the FOM is significantly improved as well. The inset of Fig. 9(b) shows the compressed pulse (black curve) and the corresponding reference pulse (red dotted curve) for the case of 64 replicas as the 1st composite plate is 6-mm in thickness. In this scenario, the FOM reaches 0.93 and the 44-fs compressed pulse has 121.1-μJ energy with 2.3-GW peak power.

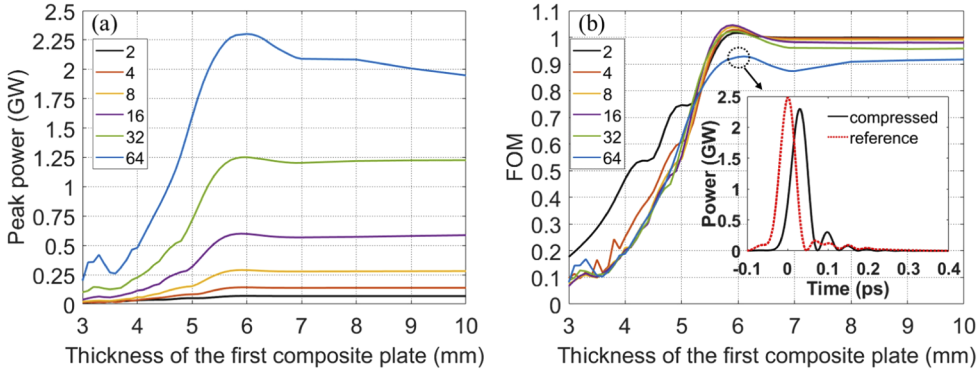

Fig. 9. (a) Peak power and (b) FOM of the compressed pulse generated by the PCM-DPA system based on composite plates for different replica numbers. Inset: the compressed pulse (black curve) and corresponding reference pulse (red dotted curve) for 64 replicas as the first composite plate is 6 mm in thickness.

The above simulation results confirm that a reduced GDD-difference improves the peak-power (and energy) scalability of a PCM-DPA system. However, due to their relatively small GD-difference, the composite plates have to be much thicker than the YVO_4 or α-BBO plates used in a PCM-DPA based on single material birefringent plates. The results in Fig. 9 shows that

Optics EXPRESS

the first composite plate needs to be at least 6-mm thick in order to provide adequate replica interval. The final composite plate is 9.6-cm (19.2-cm) in thickness for 32 (64) replicas and the total thickness of the divider/combiner reaches at least 18.6 cm (37.8 cm), which compromises the system compactness. It is noteworthy that, for the single-material divider/recombiner, the plate with the largest thickness results in the GDD difference more than that generated by all other plates combined. Therefore we propose a hybrid divider/recombiner design, in which we only replace the thickest single-material plate by a composite plate that provides the same amount of GD difference; see the illustration by the inset of Fig. 10(a). Figure 10 shows the peak power [Fig. 10(a)] and FOM [Fig. 10(b)] of the compressed pulse for 32 and 64 replicas based on the mixture of α-BBO plates and a composite plate. The insets in Fig. 10(b) correspond to the compressed pulses with the highest peak power and FOM, respectively. For 32 replicas, the maximum peak power of 1.13 GW (corresponding to a FOM of 0.96) is obtained as the first α-BBO is 2.8 mm in thickness (black curve in Fig. 10). It is close to the highest peak power of 1.25 GW obtained using 32 replicas when pure composite plates are employed (green curve in Fig. 9), but the total thickness of the divider/recombiner in the hybrid design is reduced to 13.6 cm. Even for the case of 64 replicas, the hybrid design results in a maximum peak power of 1.84 GW with an acceptable FOM of 0.73 (red curve in Fig. 10); the divider/recombiner thickness is 26.5 cm.

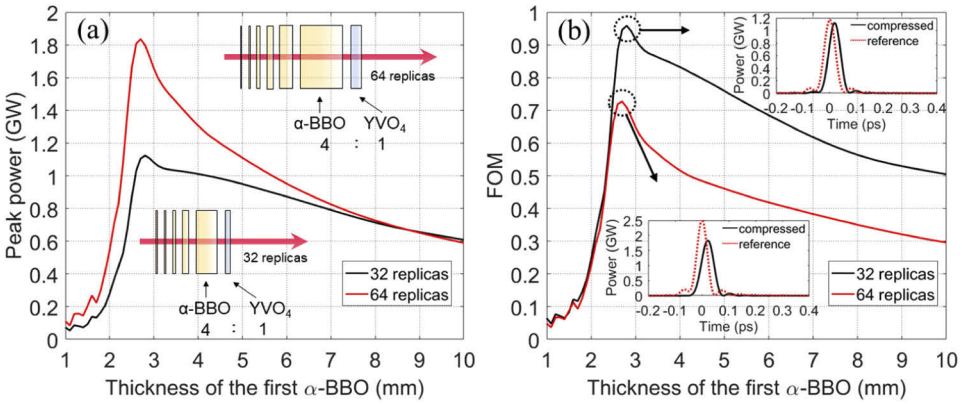

Fig. 10. (a) Peak power and (b) FOM of the compressed pulse generated by the PCM-DPA system based on a hybrid design of the divider/recombiner.

5. Discussion and conclusion

During the coherent combining, the peak-power of the recombined pulse from 64 replicas based on composite plates is ~64 MW, which exceeds the critical peak power of self-focusing. For a collimated Gaussian beam entering the crystal with a 3-mm beam diameter, the self-focusing distance is estimated to be >5 m, much larger than the thickness of the birefringent plates in the divider/recombiner. Therefore self-focusing is negligible for pulse combining in the proposed Yb-fiber PCM-DPA system.

As for experimental implementation, Fig. 1 represents one possible configuration, which adopts separate divider/recombiner stages together with a single-pass Yb-fiber amplifier. To prevent detrimental effects caused by environmental disturbances, an active stabilization loop might be necessary to render accurate divider/recombiner match for achieving long-term stability. An alternative configuration is to use one set of birefringent plates followed by a double-pass Yb-fiber amplifier. In this scenario, the same set of plates serves as both the divider and recombiner and, therefore, active stabilization is unnecessary.

Optics EXPRESS

To conclude, we numerically analyze the energy (and peak power) scalability of Yb-fiber PCM-DPA system. To better evaluate the system performance, we define a new FOM that is directly related to the peak power of the compressed quality. To mitigate the adverse effect of that GDD difference associated with the single-material birefringent plates, we propose dual-material (i.e., YVO_4 and α-BBO) composite plates featuring negligible GDD in a broad wavelength range. We explicitly show that using these composite plates to construct the divider/recombiner in a PCM-DPA system ensures an excellent energy (and peak power) scalability. Such a system employing 64 pulse replicas can deliver 121-μJ, 44-fs pulses with 2.3-GW peak power. To reduce the overall thickness of composite-plate based divider/recombiner, we further provide a hybrid design which can generate 61-μJ, 48-fs pulses with 1.13-GW peak power. Compared with current Yb-fiber PCMA systems, these results represent one order of magnitude improvement in terms of pulse energy and peak power. Although our investigation focuses on Yb-fiber PCM-DPA systems, the proposed idea of composite plates and hybrid design can be applied to nonlinear pulse compression and other nonlinear amplification techniques (e.g., parabolic pulse amplification and gain-managed amplification).

Funding. Guangdong Key R&D Program (2018B090904003); National Natural Science Foundation of China (11774234); Chinese Academy of Sciences (YJKYYQ20190034).

Acknowledgment. We thank Prof. Zhiyi Wei of Institute of Physics CAS for useful discussions.

Disclosures. The authors applied for a patent based on part of the results in this paper.

References

1. G. Q. Chang and Z. Y. Wei, "Ultrafast fiber lasers: an expanding versatile toolbox," iScience **23**(5), 101101 (2020).
2. A. Tünnermann, J. Limpert, and S. Nolte, "Ultrashort pulse fiber lasers and amplifiers," Topics in Applied Physics **96**, 35–54 (2004).
3. M. E. Fermann and I. Hartl, "Ultrafast fibre lasers," Nat. Photonics **7**(11), 868–874 (2013).
4. M. N. Zervas and C. A. Codemard, "High power fiber lasers: a review," IEEE J. Sel. Top. Quantum Electron. **20**(5), 219–241 (2014).
5. F. Röser, T. Eidam, J. Rothhardt, O. Schmidt, D. N. Schimpf, J. Limpert, and A. Tünnermann, "Millijoule pulse energy high repetition rate femtosecond fiber chirped-pulse amplification system," Opt. Lett. **32**(24), 3495–3497 (2007).
6. J. Limpert, T. Schreiber, T. Clausnitzer, K. Zöllner, H.-J. Fuchs, E.-B. Kley, H. Zellmer, and A. Tünnermann, "High-power femtosecond Yb-doped fiber amplifier," Opt. Express **10**(14), 628–638 (2002).
7. D. N. Papadopoulos, Y. Zaouter, M. Hanna, F. Druon, E. Mottay, E. Cormier, and P. Georges, "Generation of 63 fs 4.1 MW peak power pulses from a parabolic fiber amplifier operated beyond the gain bandwidth limit," Opt. Lett. **32**(17), 2520–2522 (2007).
8. Y. Deng, C.-Y. Chien, B. G. Fidric, and J. D. Kafka, "Generation of sub-50 fs pulses from a high-power Yb-doped fiber amplifier," Opt. Lett. **34**(22), 3469–3471 (2009).
9. B. Nie, D. Pestov, F. W. Wise, and M. Dantus, "Generation of 42-fs and 10-nJ pulses from a fiber laser with self-similar evolution in the gain segment," Opt. Express **19**(13), 12074–12080 (2011).
10. H.-W. Chen, J. Lim, S.-W. Huang, D. N. Schimpf, F. X. Kärtner, and G. Chang, "Optimization of femtosecond Yb-doped fiber amplifiers for high-quality pulse compression," Opt. Express **20**(27), 28672–28682 (2012).
11. J. Lim, H.-W. Chen, G. Chang, and F. X. Kärtner, "Frequency comb based on a narrowband Yb-fiber oscillator: pre-chirp management for self-referenced carrier envelope offset frequency stabilization," Opt. Express **21**(4), 4531–4538 (2013).
12. J. Zhao, W. Li, C. Wang, Y. Liu, and H. Zeng, "Pre-chirping management of a self-similar Yb-fiber amplifier towards 80 W average power with sub-40 fs pulse generation," Opt. Express **22**(26), 32214–32219 (2014).
13. W. Liu, D. N. Schimpf, T. Eidam, J. Limpert, A. Tunnermann, F. X. Kartner, and G. Chang, "Pre-chirp managed nonlinear amplification in fibers delivering 100 W, 60 fs pulses," Opt. Lett. **40**(2), 151–154 (2015).
14. Y. Liu, W. Li, D. Luo, D. Bai, C. Wang, and H. Zeng, "Generation of 33 fs 93.5 W average power pulses from a third-order dispersion managed self-similar fiber amplifier," Opt. Express **24**(10), 10939–10945 (2016).
15. D. Luo, W. Li, Y. Liu, C. Wang, Z. Zhu, W. Zhang, and H. Zeng, "High-power self-similar amplification seeded by a 1 GHz harmonically mode-locked Yb-fiber laser," Rev. Sci. Instrum. **87**(9), 093114 (2016).
16. H. Song, B. Liu, Y. Li, Y. Song, H. He, L. Chai, M. Hu, and C. Wang, "Practical 24-fs, 1-μJ, 1-MHz Yb-fiber laser amplification system," Opt. Express **25**(7), 7559–7566 (2017).
17. D. Luo, Y. Liu, C. Gu, C. Wang, Z. Zhu, W. Zhang, Z. Deng, L. Zhou, W. Li, and H. Zeng, "High-power Yb- fiber comb based on pre-chirped-management self-similar amplification," Appl. Phys. Lett. **112**(6), 061106 (2018).
18. Y. Hua, G. Chang, F. X. Kartner, and D. N. Schimpf, "Pre-chirp managed, core-pumped nonlinear PM fiber amplifier delivering sub-100-fs and high energy (10 nJ) pulses with low noise," Opt. Express **26**(5), 6427–6438 (2018).

Optics EXPRESS

19. Y. Zhang, R. Z. Chen, H. D. Huang, Y. Z. Liu, H. Teng, S. B. Fang, J. L. Wang, J. F. Zhu, G. Q. Chang, and Z. Y. Wei, "Pre-chirp managed amplification of circularly polarized pulses using chirped mirrors for pulse compression," OSA Continuum **3**(7), 1988 (2020).
20. P. Sidorenko, W. Fu, and F. Wise, "Nonlinear ultrafast fiber amplifiers beyond the gain-narrowing limit," Optica **6**(10), 1328 (2019).
21. P. Sidorenko and F. Wise, "Generation of 1 μJ and 40 fs pulses from a large mode area gain-managed nonlinear amplifier," Opt. Lett. **45**(14), 4084–4087 (2020).
22. F. Guichard, M. Hanna, Y. Zaouter, D. N. Papadopoulos, F. Druon, and P. Georges, "Analysis of limitations in divided-pulse nonlinear compression and amplification," IEEE J. Sel. Top. Quantum Electron. **20**(5), 619–623 (2014).
23. H. Tu, Y. Liu, J. Laegsgaard, D. Turchinovich, M. Siegel, D. Kopf, H. Li, T. Gunaratne, and S. A. Boppart, "Nonlinear polarization dynamics in a weakly birefringent all-normal dispersion photonic crystal fiber: toward a practical coherent fiber supercontinuum laser," Opt. Express **20**(2), 1113–1128 (2012).
24. L. M. Frantz and J. S. Nodvik, "Theory of pulse propagation in a laser amplifier," J. Appl. Phys. **34**(8), 2346–2349 (1963).
25. S. Zhou, F. W. Wise, and D. G. Ouzounov, "Divided-pulse amplification of ultrashort pulses," Opt. Lett. **32**(7), 871–873 (2007).
26. L. J. Kong, L. M. Zhao, S. Lefrancois, D. G. Ouzounov, C. X. Yang, and F. W. Wise, "Generation of megawatt peak power picosecond pulses from a divided-pulse fiber amplifier," Opt. Lett. **37**(2), 253–255 (2012).
27. L. Daniault, M. Hanna, D. N. Papadopoulos, Y. Zaouter, E. Mottay, F. Druon, and P. Georges, "High peak-power stretcher-free femtosecond fiber amplifier using passive spatio-temporal coherent combining," Opt. Express **20**(19), 21627–21634 (2012).
28. F. Guichard, Y. Zaouter, M. Hanna, F. Morin, C. Hönninger, E. Mottay, F. Druon, and P. Georges, "Energy scaling of a nonlinear compression setup using passive coherent combining," Opt. Lett. **38**(21), 4437–4440 (2013).
29. A. Klenke, M. Kienel, T. Eidam, S. Hädrich, J. Limpert, and A. Tünnermann, "Divided-pulse nonlinear compression," Opt. Lett. **38**(22), 4593–4596 (2013).
30. D. Wang, Y. Leng, and Z. Huang, "Divided-pulse compression with gas-filled hollow-core fiber for generation of high-energy few-cycle pulses," J. Opt. Soc. Am. B **31**(6), 1248–1254 (2014).
31. E. S. Lamb, L. G. Wright, and F. W. Wise, "Divided-pulse lasers," Opt. Lett. **39**(9), 2775–2777 (2014).
32. Q. Hao, Q. Zhang, T. Sun, J. Chen, Z. Guo, Y. Wang, Z. Guo, K. Yang, and H. Zeng, "Divided-pulse nonlinear amplification and simultaneous compression," Appl. Phys. Lett. **106**(10), 101103 (2015).
33. Q. Hao, Y. F. Wang, T. T. Liu, H. Hu, and H. Zeng, "Divided-pulse nonlinear amplification at 1.5 μm," Appl. Phys. Lett. **106**(10), 101103 (2015).
34. H. Jacqmin, B. Mercier, A. Jullien, and R. Lopez-Martens, "Manifold coherent combining of few-cycle pulses in hollow-fiber compressors," Appl. Phys. B **122**(8), 218 (2016).